WP3 - Irradiation test plans

A few target applications have been proposed for ASPIDES devices, particularly in accelerator-based experiments. These include both calorimetry and Cherenkov particle identification (PID) detectors. WP3 will carry out radiation damage tests on ASPIDES devices to assess their suitability for radiation harsh environments in collider experiments and to provide input on fundamental damage mechanisms.

This is conceived as a living document, aimed at continuously updating the state of the art and outlining the irradiation strategies and planning.

Table of Contents

- 1 State of the art
 - o 1.1 Displacement damage
 - 1.2 Ionizing damage
 - 1.3 Bibliography
- 2. Irradiation test
 - 2.1 Test with protons
 - 2.2 Test with xrays
 - o 2.3 others

1. State of the art

Geiger-mode silicon devices are known to be highly sensitive to bulk damage, making the evaluation of their radiation tolerance essential. Displacement of silicon atoms due to non-ionizing radiation creates bulk defects that can interact with each other or with dopants in the material. These defects generate charge carriers, increasing the dark count rate (DCR) through thermal Shockley–Read–Hall (SRH) processes or electric-field-assisted mechanisms. Metastable defects introduced during irradiation can result in discrete switching of the DCR between two or more levels, with characteristic timescales of several seconds. This phenomenon is known as Random Telegraph Signal (RTS).

lonizing radiation damage is generally not the most critical issue for CMOS SPADs, especially when compared to bulk damage mechanisms.

1.1 Displacement Damage Studies

Several irradiation campaigns have been conducted on CMOS SPADs as part of various INFN R&D efforts. Tests with both protons and neutrons have shown significant DCR degradation and the emergence of RTS effects.

1.1.1 DCR increase

In [Campajola_2019_NIMA] authors studied 150 nm CMOS SPADs irradiated with around 20 MeV protons at the LNS Tandem laboratory. Devices exhibited typical pre-irradiation DCR values in the kHz range for 10x10 \mum^2 SPADs. Two layouts were tested: PWNISO and PNWELL. Several samples have been irradiated, and degradation trends were measured post-irradiation. An almost linear trend as a function of the dose has been measured. At a maximum dose of 600 TeV/g (corresponding to ~3×10¹¹ n_eq/cm²), a median DCR of 200

kcps (corresponding to 2 GHz/mm2) was measured. Values refers to measurement permed one month after the irradiation, when prompt annealing effects finished.

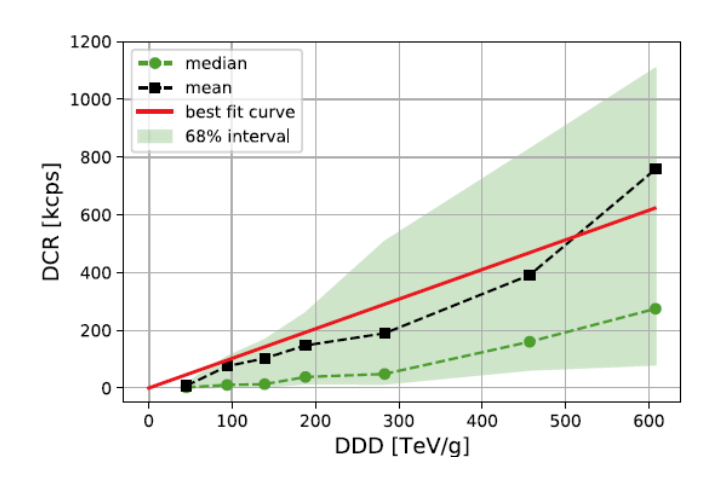


Figure. DCR increase on 10x10 \mum^2 SPADs as a function of the displacement damage dose delivered with 20 MeV protons at the LNS Tandem. From [Campajola_2019]

Several irradiation campaigns with neutrons were carried out by the APIX and ASAP collaborations. These were performed at LNL using Be-target 5 MeV proton-induced reactions. Typical spectrum of neutron energy is reported in Figure.

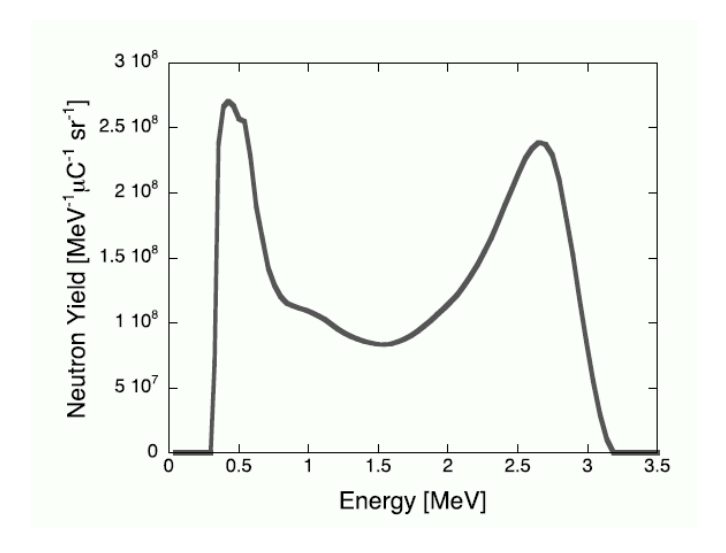


Figure. Distribution of the neutron yield of the INFN Laboratori Nazionali di Legnaro source at a 0° emission angle

In [Ratti_2019_TNS], authors irradiated a 180 nm CMOS SPAD device with P+NWELL structures. The initial DCR was of ~MHz/mm². After irradiation up to 1E11 n_eq/cm2 values and a standard thermal annealing procedure at 60°C for 80 minutes, DCRs reached values on the order [0.1, 1] GHz/mm².

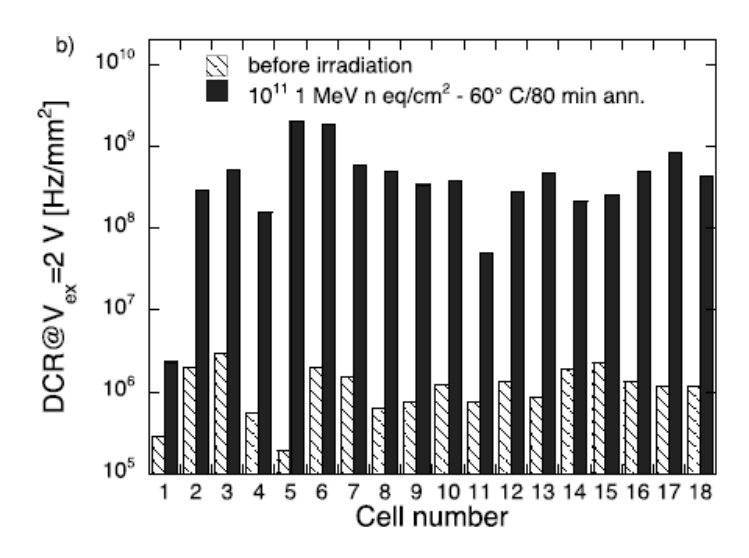


Figure. DCR at an excess voltage of 2 V normalized to the active area for a sensor exposed to 1E11 1-MeV neutron equivalent cm-2. From [Ratti_2019_TNS]

In [Ficorella_2019_phd], results of irradiation with neutrons on 150 nm APIX chips. They irradiated several devices and characterised DCR in steps during the irradiation campaign, and after a standard annealing procedure heating devices at 60°C for 80min. The mean DCR as a function of the neutron fluence up to a fluence of 1E11 n_eq/cm2 exhibits a linear dependence with the fluence.

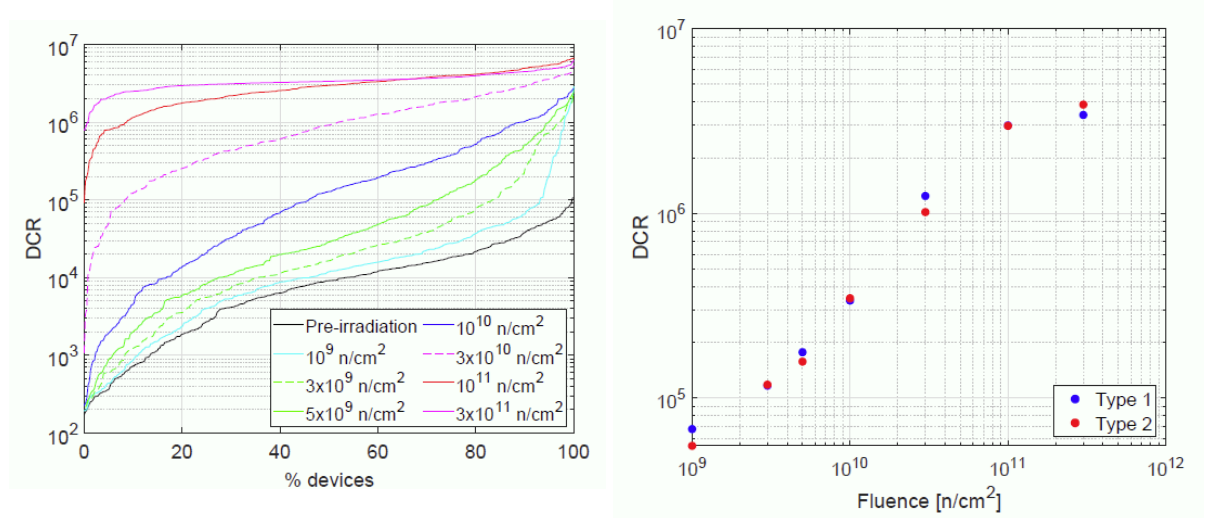


Figure. DCR distributions for SPAD samples irradiated at different neutron fluences. VEX = 1V at room temperature. From [Ficorella_2019_phd]

The comparison of the DCR distributions of two different irradiated devices before and after annealing is reported as well.

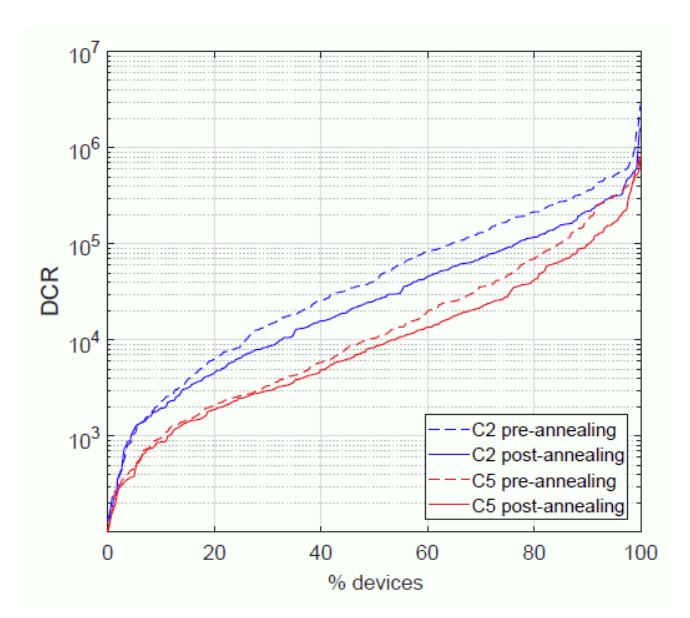


Figure: DCR distributions of two devices before and after the annealing procedure. From [Ficorella_2019_phd]

In [Ratti_2019_TED] with a fluence of 1E11 n_eq/cm2, a DCR increase on the 150nm devices of 5E6 Hz on SPADs of 50x50\mum2 is reported, corresponding to 2 GHz/mm2.

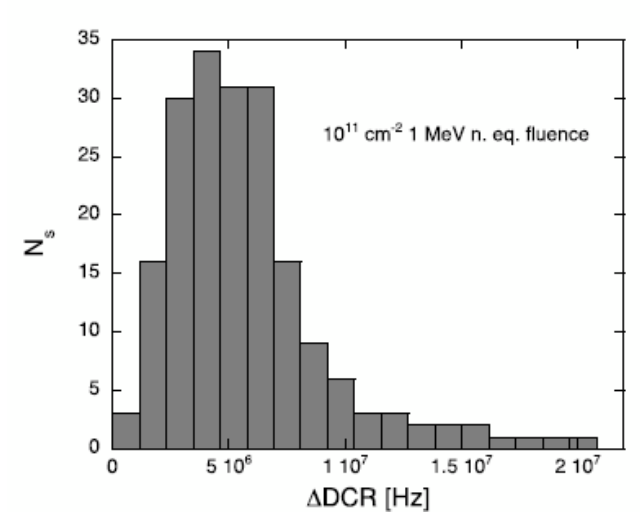


Figure. Distribution of the DCR increase in a population of 192 type 1 SPADs with 43 \times 45 μ m2 active area after exposure to a 1-MeV neutron equivalent fluence of 1011 cm-2. From [Ratti_2019_TED]

1.1.2 Online DCR

During the APIX/ASAP collaboration tests, online measurements of the Dark Count Rate (DCR) were also performed during irradiation. Monitoring the DCR in real time is a valuable tool to study the dynamics of defect formation and short-term annealing processes.

In [Ficorella_2019_phd], a test with a micro-beam of protons at LNL on a 180 nm chip is reported. During irradiation, the DCR exhibits sudden step-like increases. These can be attributed to the formation of clusters of defects along the trajectory of a primary knock-on

atom, dislodged by scattering with an incoming beam particle. The step-like behaviour, interspersed with long periods without any DCR increase, can be explained by the stochastic nature of defect generation and the relatively low cross section for such interactions.

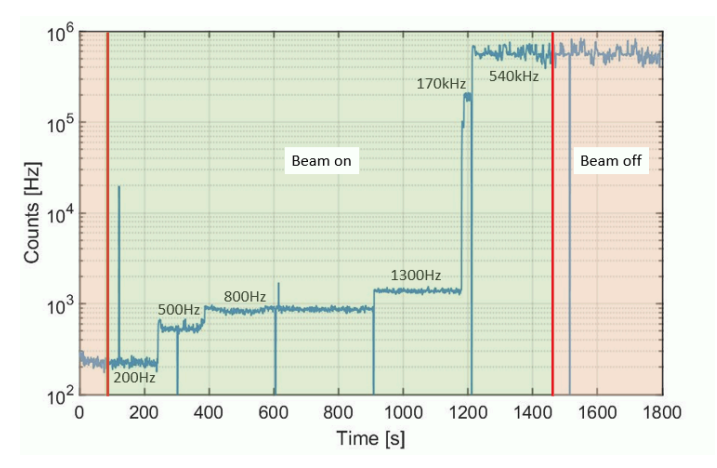


Figure. Output signal of a pixel detector under proton irradiation. From [Ficorella 2019 phd].

In [Ratti_2024_TNS] authors also performed online DCR measurements during irradiation with neutrons, on a 150 nm chip. They monitored a subset of around 100 SPADs with a time sampling of 100 ms. Online measurements of the DCR revealed a range of different behaviors, including the time evolution of the DCR after the neutron hit was responsible for defect creation. A fast recovery, taking place over a single 100 ms step (corresponding to the time resolution used in the acquisition) can be observed. This is followed by a much slower decay with an incomplete recovery as compared to the prior DCR level. The slow time constant is about 9s, and the delta DCR induced by the hit is reported to be some 10 kHz.

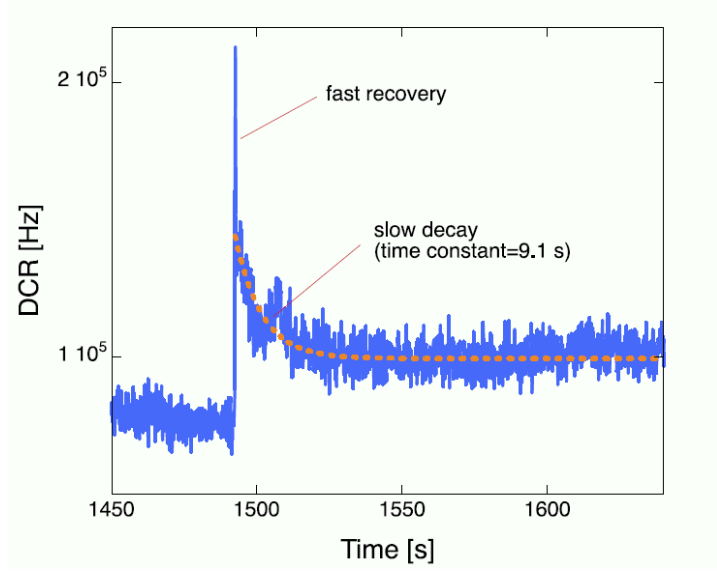


Figure. DCR as a function of time for a SPAD during neutron irradiation. From [Ratti_2024_TNS]

1.1.3 Breakdown Voltage Stability

The effect of radiation damages on the breakdown voltage was evaluated by performing a voltage sweep and measuring the DCR for each voltage value. In all these tests no significant change in breakdown voltage was observed after neutron or proton irradiation up to 1E11 n_eq/cm2.

Only In [Ficorella_2019_phd], reported a detailed study, showing a reduction of the breakdown voltage in the order of a few tens of mV, while the annealing does not affect its value.

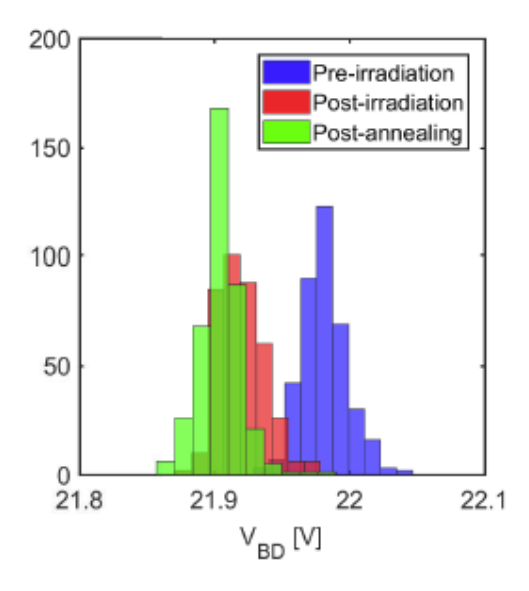


Figure. Histograms of the breakdown voltage for before and after the irradiation. From [Ficorella_2019_phd].

1.1.4 Activation energy

The activation energy allows one to obtain the energy trap-level information and if electric field enhancement effects are predominant.

A useful way to display the activation energies is by representing it as a function of the DCR. In [dicapua_2021_SCIREP] used this tool to assess differences among SPADs layout before irradiation.

In [Shojaei_2025_TNS] activation energy before and after irradiation with neutron in 150-nm CMOS devices have been performed. Before irradiation, distinct behaviors are observed. High-DCR pixels show a single, relatively low Ea across all temperatures, suggesting field-enhanced generation mechanisms like Poole–Frenkel and trap-assisted tunneling (TAT). Low-DCR pixels exhibit two distinct Ea values: near the silicon bandgap at high temperatures (carrier injection dominant) and near zero at low temperatures (band-to-band tunneling, BTBT).

After irradiation, a single Ea can typically be extracted across the full temperature range, indicating reduced temperature dependence, i.e. field assisted mechanisms being the dominant generation mechanism.

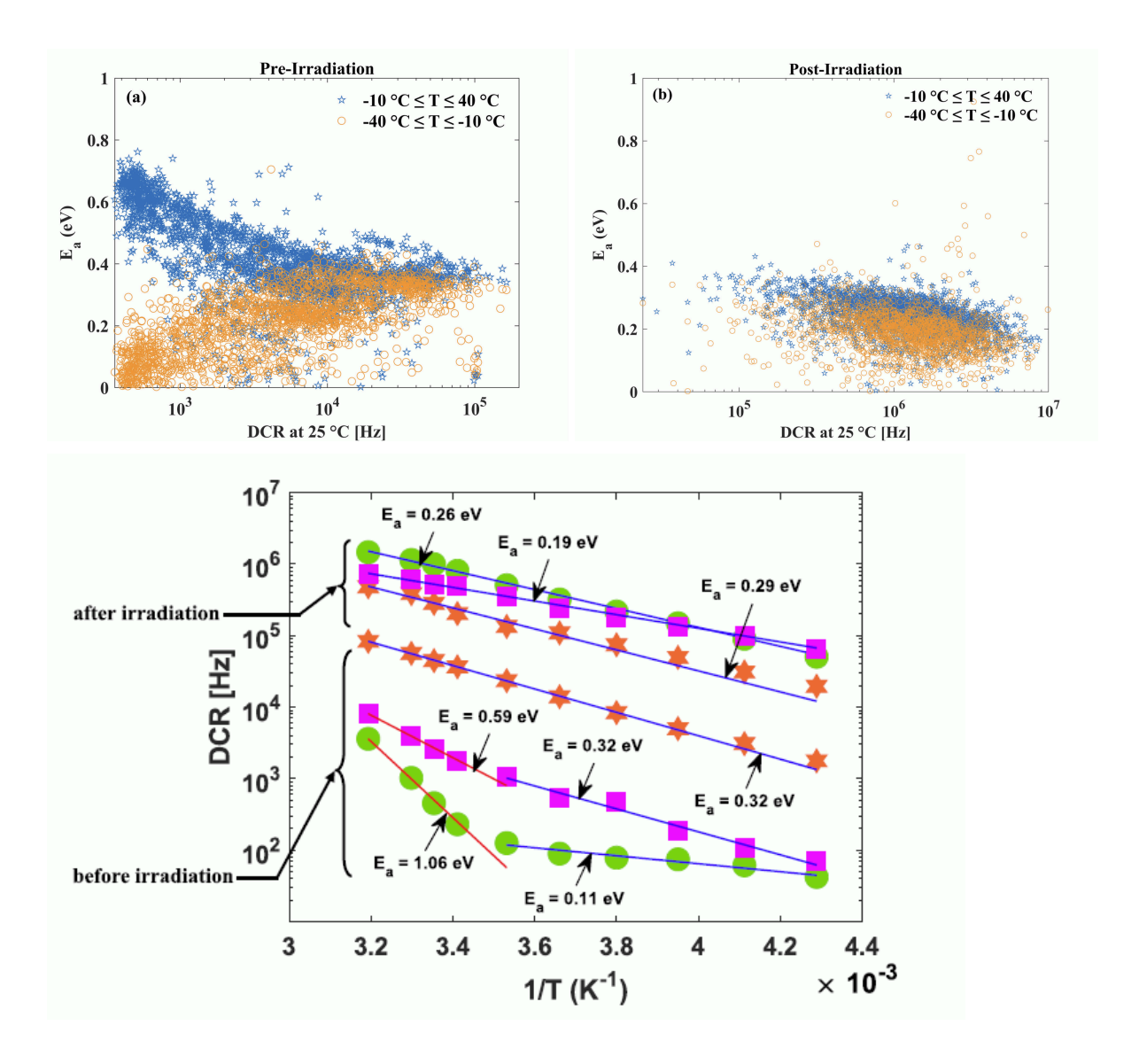


Figure. Activation energy distribution versus DCR at 25 $^{\circ}$ C for two temperature domains: -40 $^{\circ}$ C $^{\circ}$ C $^{\circ}$ C and -10 $^{\circ}$ C $^{\circ}$ C before irradiation and after exposure to an integrated fluence of 4.15 × 1010 1-MeV neg cm-2. From [Shojaei 2025 TNS]

1.1.5 Temperature annealing damage recovery

High temperature, isochronal annealing techniques can be used to investigate the nature of the defects involved in radiation-induced DCR increase.

In [Campajola_2019_NIMA] authors explored thermal annealing in steps of 50 degree per run with 1h permanence in the oven. A strong recovery effect was observed at temperatures around 150 °C. The non-sharp observed decrease could be attributed to the combination of different types of defects with different annealing temperature or due to a strong contribution from cluster defects. According to the literature, the defects corresponding to the observed annealing temperature interval are dopant related vacancy complexes as V-P.

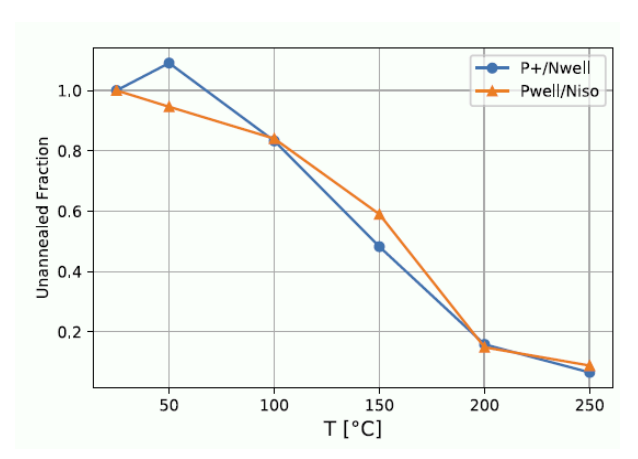


Figure. Evolution of unannealed fraction of DCR as a function of the annealing temperature step on proton irradiated SPADs at a DDD = 608 TeV/g. From [Campajola 2019 NIMA]

1.1.6 Random Telegraph Signal (RTS)

Random Telegraph Signal (RTS) effects on the DCR have been observed in a significant number of studies following proton and neutron irradiation. [dicapua_2018_TNS, dicapua_2021_SCIREP, ficorella_2019_phd,Ratti_2024_TNS]

These effects differ from the classical RTS behavior seen in MOSFETs. In SPADs, RTS can arise from metastable defects capable of switching among multiple steady-state configurations, each associated with a distinct increase in the DCR.

In [dicapua_2018_TNS, dicapua_2021_SCIREP] authors investigated the dependence on layout and dose, finding a higher incidence in sharp profile junctions, i.e. PNWELL layouts compared to PWNISO. They also studied RTS activation energy and annealing behavior, consistently pointing to the involvement of P-V centers in RTS formation. The fraction of SPADs with RTS features in their DCR was found to increase with the displacement damage dose and to recover almost completely after isochronal, high temperature annealing up to 250 °C

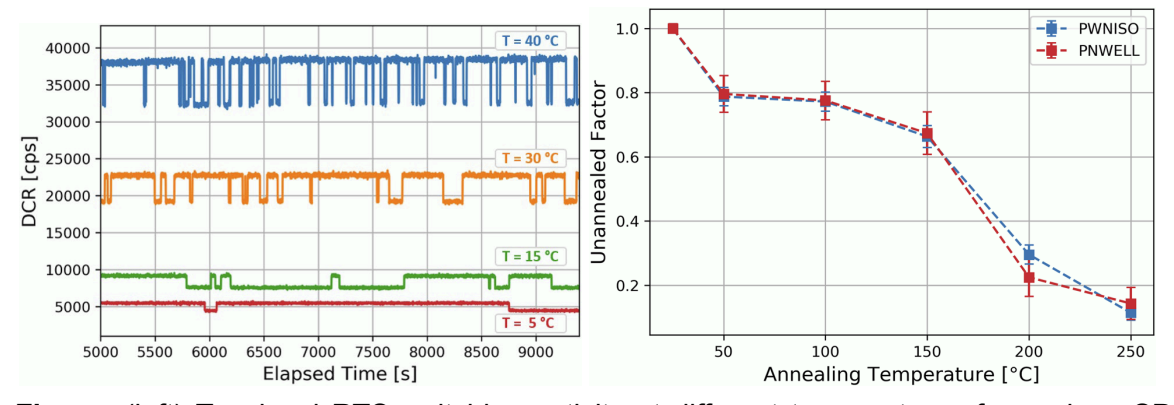


Figure. (left) Two-level RTS switching activity at different temperatures for a given SPAD, (right) evolution of the remaining RTS pixels for different annealing steps. From [dicapua_2021_SCIREP].

1.1.7 Test with electrons and NIEL scaling

The Non-Ionizing Energy Loss (NIEL) scaling hypothesis assumes that radiation-induced damage is proportional to the non-ionizing energy deposited.

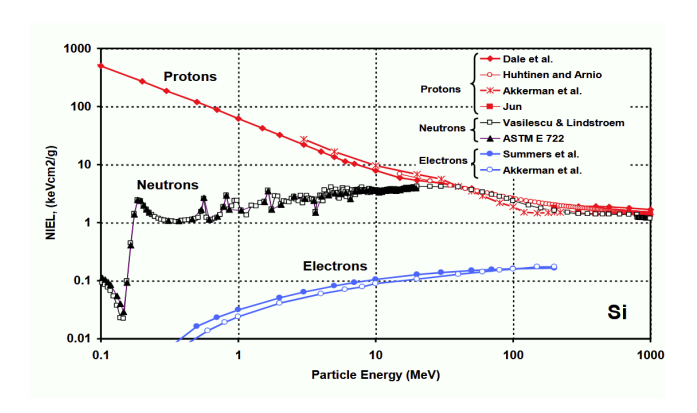


Figure. NIEL. From RD48 curve.

However, this approach does not account for the differences between point defects and cluster damage. Identical NIEL values can result in different microscopic damage profiles. Deviations from linear scaling have already been reported in several studies.

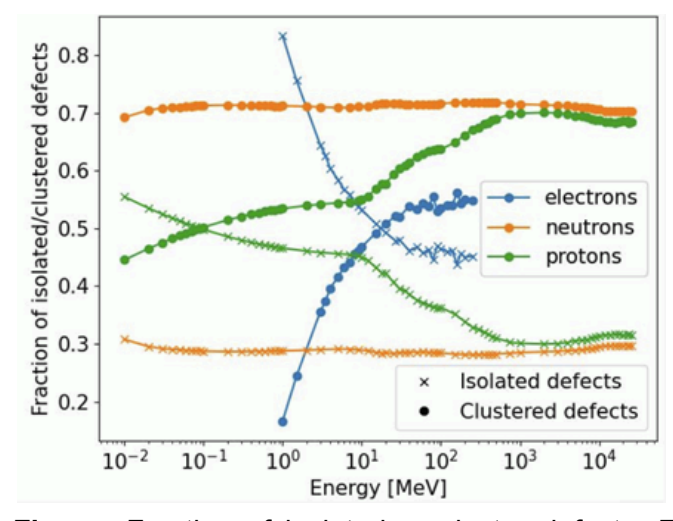


Figure: Fraction of isolated or cluster defects. From V. Maulerova-Subert, I. Dawson, E. Garutti, M.Moll, NIEL(non-ionizing energy loss) Simulations and displacement damage studies towards a more complex NIEL concept for radiation damage modelling and prediction

Di Capua, Campajola et al. also irradiated the same devices using 2 MeV electrons. While MeV electrons primarily induce isolated point-like defects, 20 MeV protons tend to generate clusters of defects. In [Campajola_2020_SPIE], authors compared to protons, electron irradiation resulted in a smaller increase in DCR.

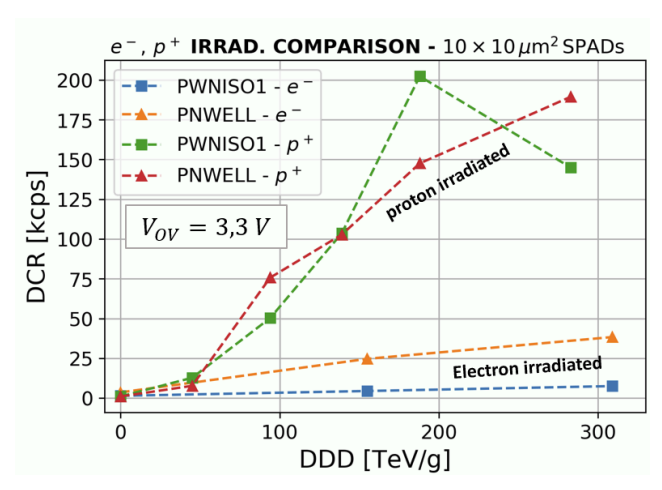


Figure. DCR evolution as a function of the dose for 20 MeV proton and 2 MeV electron irradiations. From [Campajola_2020_SPIE].

Also DCR distributions for proton irradiation led to a significant spread in the DCR values across the SPAD population, whereas electron irradiation resulted in smaller spread of values. These differences are attributed to the much lower likelihood of cluster defect formation from electron interactions, as opposed to the more damaging effects of 20 MeV protons.

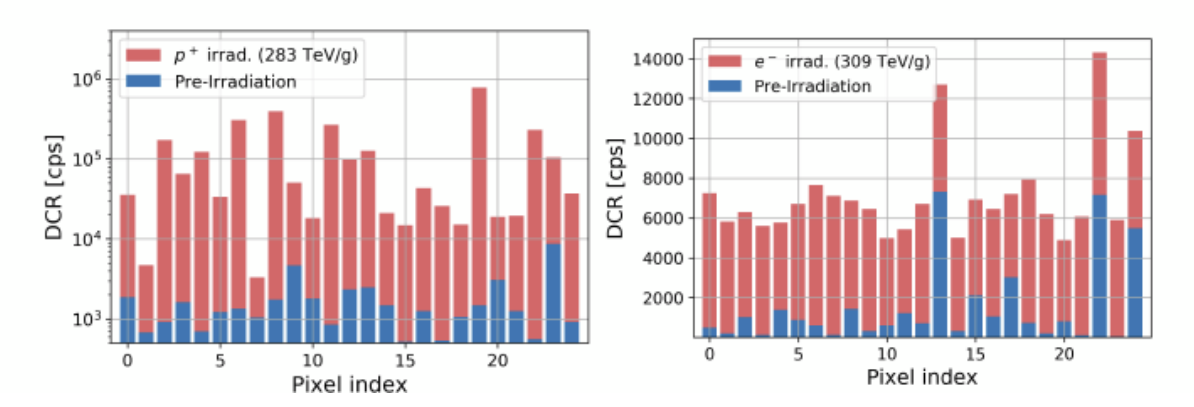


Figure. DCR before and after irradiation with 20 MeV proton and 2 MeV electron. From [Campajola_2020_SPIE].

1.2 lonizing damage

lonization-induced damage, caused by charge build-up in oxide layers, is known to be strongly dependent on the specific CMOS technology. Ionizing radiation damage is generally not the most critical issue for CMOS SPADs, especially when compared to bulk damage mechanisms. However, it remains important to study how device performance evolves with increasing radiation dose.

1.2.1 X-rays

In Ratti_2019_TNS, authors irradiated devices using a 10 keV, RP-149 X-ray Semiconductor Irradiation System from Seifert available at Padova. The maximum dose was 1 Mrad(SiO2). At the maximum dose an average DCR increase of slightly less than 30%, from about 250

kHz/mm2 to about 320 kHz/mm2, at low/moderate bias voltage was observed. Up to the 1-Mrad(SiO2) dose authors didn't observe appreciably change in the breakdown voltage. However, when Vbd gets above 24 V, a much steeper increase in the DCR is observed in irradiated devices. Authors interpreted the underlying mechanism as related to a radiation-induced breakdown phenomenon in a secondary junction, such as the HV PW/NW one, in the region close to the shallow trench isolation oxide (STI). Radiation-induced charge accumulation in the STI, as well as increase in trap density at or close to the Si/SiO2 interface, may be responsible for a reduction of the breakdown voltage at that junction, leading to the observed sharp increase in DCR.

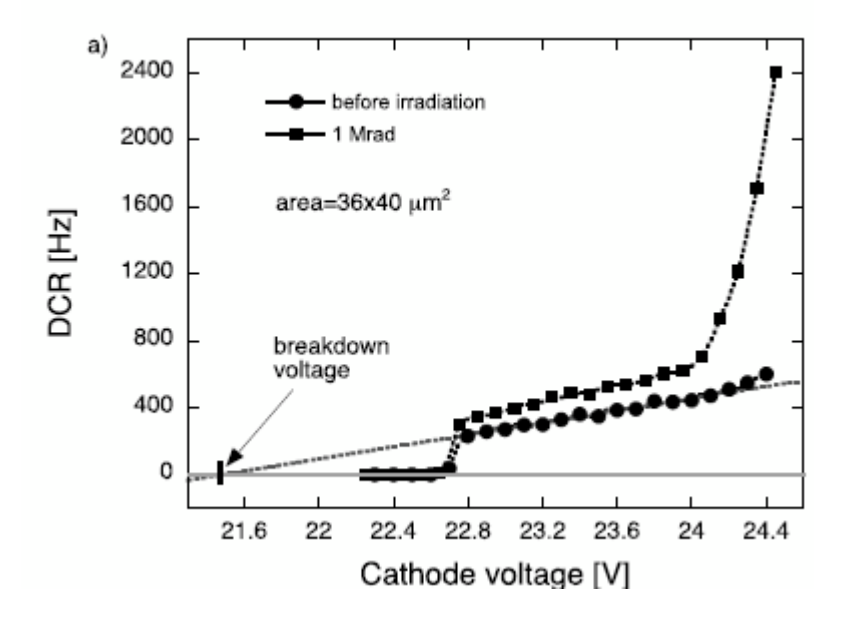


Figure. DCR as a function of the voltage applied to the SPAD cathode before irradiation and after exposure to a 1-Mrad(SiO2) total ionizing dose. From [Ratti 2019 TNS]

1.3 Bibliography

- [Campajola_2019_NIMA] M. Campajola *et al.*, "Proton induced dark count rate degradation in 150-nm CMOS single-photon avalanche diodes," *Nuclear Instruments and Methods in Physics Research Section A*, 2019.
- [Ratti_2019_TNS] L. Ratti, P. Brogi, G. Collazuol, G.-F. Dalla Betta, A. Ficorella, L. Lodola *et al.*, "Dark Count Rate Degradation in CMOS SPADs Exposed to X-Rays and Neutrons," *IEEE Transactions on Nuclear Science*, vol. 66, no. 2, pp. 567–574, Feb. 2019. DOI: 10.1109/TNS.2019.2893233.
- [Ficorella_2019_phd] A. Ficorella, Application of Avalanche Detectors in Scientific and Industrial Measurement Systems, PhD Thesis, Università di Trento, 2019.
- [Ratti_2024_TNS] L. Ratti, P. Brogi, G. Collazuol, G.-F. Dalla Betta, J. C. Delgado, P. S. Marrocchesi *et al.*, "Online Dark Count Rate Measurements in 150 nm CMOS

SPADs Exposed to Low Neutron Fluxes," *IEEE Transactions on Nuclear Science*, vol. 71, no. 4, pp. 698–707, Apr. 2024. DOI: 10.1109/TNS.2024.3353689.

- [dicapua_2021_scirep] F. Di Capua, M. Campajola, L. Gasperini *et al.*, "Investigation of random telegraph signal in two junction layouts of proton irradiated CMOS SPADs," *Scientific Reports*, vol. 11, 2021.
- [Campajola_2020_SPIE] M. Campajola, F. Di Capua, L. Gasperini, "Comparison of proton and electron radiation effects on dark count rate in a CMOS SPAD sensor," *Proc. SPIE 11454, X-Ray, Optical, and Infrared Detectors for Astronomy IX*, 1145409, 13 Dec. 2020. DOI: 10.1117/12.2559507.
- [dicapua_2018_TNS] F. Di Capua, M. Campajola, L. Gasperini, and M. Ambrosio, "Random Telegraph Signal in Proton Irradiated CMOS SPADs," *IEEE Transactions on Nuclear Science*, vol. 65, no. 8, pp. 1986–1993, Aug. 2018. DOI: 10.1109/TNS.2018.2840691.
- [Shojaei_2025_TNS] F. Shojaei "Bulk Damage Effects in Neutron Irradiated Singleand Dual-Layer 150-nm CMOS SPADs" IEEE TRANSACTIONS ON NUCLEAR SCIENCE, VOL. 72, NO. 3, MARCH 2025

2. Irradiation tests

Among calorimetric applications, dual-readout calorimetry based on fiber detectors at the FCC-ee collider is a key target. This environment features relatively moderate radiation levels, thanks to the lepton collider configuration and the detector's location far from the interaction point (IP), where it is also shielded by a significant material budget. FLUKA simulations indicate a maximum fluence below 10¹⁰ n_eq/cm² per year and a total ionizing dose (TID) of less than 10 Gy/year [FCC study link]

Conversely, Cherenkov imaging detectors are located closer to the IP and generally lack effective shielding, resulting in significantly higher radiation exposure. These detectors also impose stricter constraints on dark count rate (DCR) performance. For this reason, even fluences on the order of 10¹¹ n_eq/cm² may cause SPADs to fall out of specification unless periodic damage recovery techniques are applied.

Given this, and considering that previous studies have shown DCR values approaching the GHz/mm² range at fluences of ~10¹¹ n_eq/cm², we consider it unnecessary to test devices beyond this radiation level.

While ionizing radiation damage is generally less critical for CMOS SPADs compared to bulk damage mechanisms, it is still important to assess how device performance evolves with increasing dose. Thus doses up to the Mrad (100kGy) will be tested.

2.1 Test with protons

Deliverables include the characterization of the effects of radiation dose on key SPAD parameters such as breakdown voltage Vbd, dark count rate (DCR), afterpulsing probability, and the occurrence of Random Telegraph Signals (RTS). In addition, DCR activation energies and the potential for damage recovery through thermal annealing will be

investigated to provide insight into the nature of the radiation-induced defects.

Pre-irradiation campaigns will focus on characterizing the dependence of DCR on bias voltage and temperature. From these measurements, breakdown voltage and activation energies will be extracted.

Experimental setups are available in MI, BO and NA. The BO setup includes a climatic chamber capable of operating in the range of –40 °C to +40 °C. A climatic chamber may also be available at NA (engineering department).

Beam availability: Decembers 2025 @TIFPA

- Referente test beam: Luigi Rignanese
- Date: 11-12-13 december (still preliminary) 18:00 to 24:00 Thursday, Friday 8 to 14 on Saturday;
- Participants: L. Rignanese, F. Di Capua, M. Campajola
- Beam species: protons
- Energy accessible in the range 80 140 MeV
- Maximum flux: 5 x 10⁸ p/cm² s⁻¹
- Maximum fluence: E11 p/cm2
- beam size: 1-2 cm^2
- uniformity:

Test procedure:

Irradiation will be performed in parasite mode during ePIC SiPM tests.

We should have the beam available for one of the irradiation dates (e.g Fryday), and the chance to mount the setup before the irradiation session.

Currently we foresee to irradiate two samples:

- one of the NA samples up to the maximum fluence: 10¹11 p/cm2
- one from BO, at low-moderate doses e.g. to 10^9

At those energies the proton NIEL is almost equivalent to that of 1 MeV neutrons, thus fluence will be almost equivalent to the 1 MeV neutron equivalent. it will be quantified anyway.

The high dose (NA) chip will not be biased during the irradiation. It will be irradiated while mounted on the daughter board (and possibly on the motherboard) to facilitate the following operation of characterizations procedure.

The irradiation will be performed in steps, e.g. three steps 1E9, 5E9, 10E10, 5E10, 1E11 p/cm2.

%Running at 1E8 p/cm2, the total irradiation time is 15 min. The smaller step will last 100s. After each step, DCR measurement will be performed in situ. We will wait 100 s (enough?) after the beam off, to avoid prompt annealing effects.

During intermediate irradiation measurements the DCR will be measured on structures (A1, A2?). The procedure takes xx min to be performed.

No firmware developments are needed. Standard firmware is OK to perform these acquisitions.

The low dose chip (BO), will be irradiated while mounted on the daughter and mother boards.

Should evaluate beam size at the board level, and the necessity of shielding for ancillary components on the motherboard, but at this doses TID should be not a concern.

During the irradiation, a dedicated run with an online monitoring of the DCR during will be performed.

The proton flux ideally should be lower than the DCR density, so that induced defects could be appreciated. Potentially this could be performed on the low dose chip, during its irradiation

The DCR sampling rate per SPAD should be higher than 10 Hz to allow resolving relaxation time of defects. The interrogation time should be tuned to be sure of not saturating counters. More information on the online DCR performed by Lodovico will guide us. A dedicated firmware must be developed running on a subset of pixels.

After the end of the test, at least the high dose chip will be likely activated, and could not be bringed home immediately.

TIFPA has a refrigerator. We can ask to keep in the samples to reduce the annealing effects.

Post irradiation operations

Once back chips will be characterized in DCR vs bias.

A standard annealing procedure at 60°C for 80min will be performed to suppress short term effects and leave only permanent damage.

After that, DCR will be measured again and a scaling factor with respect to the values measured just after the irradiations will be computed and used to correct all the middle step DCR values.

DCR vs bias will be measured and V bd will be characterized.

Long acquisition will be performed to characterize RTS occurrence effects. <u>Verify which firmware to use</u>. RTS time constants are slow, so sampling rate may not be a problem.

DCR and RTS will be studied as a function of the temperature and post irradiation activation energy measurements will be performed. Both BO and NA have a climatic chamber to do that.

Finally isochronal annealing will be performed in steps of 50° for 1h cooking up to 250°. After each step, DCR and RTS (?) will be characterized, and the annealed factor curve will be obtained.

2.2 X ray irradiation

Referente: Lodovico Ratti et al.

The characterization of the test chip will include dedicated structures designed to assess the role of STI in DCR degradation under irradiation.

Measurements are planned at various total ionizing doses (TIDs), namely 100 krad, 300 krad, 1 Mrad, 3 Mrad, and 10 Mrad.

Damage is expected to be larger for biased SPADs. The chip will be irradiated with SPADs biased just below breakdown voltage to avoid continuous breakdown due to

Test plan:

- date: July 21 to 25, 2025
- facility: RP-149 X-ray Semiconductor Irradiation System by Seifert, INFN Torino
- doses: up to 10 Mrad with intermediate steps at 100 krad, 300 krad, 1 Mrad and 3 Mrad.
- dose rate: between 600 krad/h and 1 Mrad/h, depending on the distance between the edge of the X-ray tube and the DUT (to be chosen as a compromise between irradiation speed and X-ray field uniformity)

2.3 Other irradiation to be investigated

Possible irradiation campaigns of interest are:

γ-rays

 γ -rays from Co-60 besides producing cumulative ionizing effects in SiO2, create point defects in the device bulk through electrons from Compton scattering. Indeed, their energy is sufficiently high, such that these electrons may induce silicon recoils, leading to the formation of point defects only.

It's of some interest comparing the DCR degradation from Co-60 gamma with that from hadrons at the same equivalent dose, as done in [Goiffon_xx]. Differences have been observed, which suggest different role of point and cluster defects in the DCR enhancement.

As a reference, 5 krad of Co-60 γ -rays corresponds to approximately 1 TeV/g, based on the NIEL calculations by Akkerman et al.

Possible radiators with high dose rates include: Calliope @ Enea Casaccia and CC60 @ CERN.

electrons

Similarly, low energy electrons (MeV range) induce mainly point defects. Thus, it's of some interest comparing the DCR degradation from low energy with that from hadrons at the same equivalent dose, as performed in [Campajola_2020_SPIE].

A facility offering high dose rate 2 MeV electrons is in Varsaw.

alpha source (F. Di Capua)